7th International Conference on Fundamental of Adsorption, May 20-25, 2001, Nagasaki, Japan

Sorption and Phase Transitions in Nanopores

Alexander V. Neimark, Peter I. Ravikovitch, Aleksey Vishnyakov
Center for Modeling and Characterization of Nanoporous Materials
TRI/Princeton, 601 Prospect Avenue, Princeton, NJ 08542, USA
E-mail: aneimark@triprinceton.org

Abstract

We present new results on MC simulations and Density Functional Theory modeling of sorption and phase transitions in nanopores. Major attention is paid to the problems of metastability and hysteresis. It is shown that the construction of the full phase diagram, tracing continuously stable, metastable, and unstable states, sheds light on the peculiarities of equilibrium and spontaneous transitions. The proposed methods allow one to predict the adsorption isotherm, the pressure of equilibrium vapor-liquid transition, and the limits of adsorption hysteresis. Simulation and theoretical results are found to be in agreement with reference adsorption measurements.

1. Introduction

Thermodynamic properties of fluids in nanopores differ remarkably from the corresponding properties in the bulk. Nano-confined fluids are characterized by multiple metastable states and hysteretic transitions between the metastable and stable phases. The problem of theoretical description of hysteretic phase transitions during vapor sorption in porous solids has been in the center of vigorous discussions for over five decades. However, despite a number of thermodynamic and molecular simulations studies (for a recent review see ref. [1]) which have shed light on some specifics of sorption hysteresis, the origin of metastability and irreversible transitions is still poorly understood.

In this paper, we present two recently developed methods, the gauge cell Monte Carlo simulation method [2,3] and the canonical ensemble density functional theory [4]. As a prominent example we consider the capillary condensation hysteresis of nitrogen at 77 K in a cylindrical pore of 9.3 nm in diameter. The choice of system was motivated by the availability of relevant experimental data on a siliceous mesoporous molecular sieve. Nitrogen was modeled as a Lennard-Jones (LJ) fluid with the interaction parameters that provide the best fit to the experimental data on vapor–liquid equilibrium for bulk nitrogen [5]. The solid–fluid interactions were modeled by the LJ potential integrated over the cylindrical layer of adsorption centers [6] with the interaction parameters chosen to fit the adsorption isotherm on a non-porous silica. We demonstrate that both methods allow us to construct a continuous isotherm of equilibrium states forming a sigmoid curve of the van der Waals type and to determine the limits of stability of metastable states and the conditions of phase equilibrium. The results of simulations and modeling are shown to be in remarkable agreement with the experimental hysteretic capillary condensation isotherm.

2. The gauge cell method.

Construction of the continuous isotherm. To study metastable states one has to impose certain constraints to prevent density fluctuations and nucleation. The idea of the gauge cell

method is the following [2]. Simulation is performed simultaneously in two cells, which are in thermal equilibrium with an infinite heat bath, Figure 1. One of the cells represents a pore and the other is a gauge cell of a limited capacity. It is assumed that the equation of state of the fluid in the gauge cell is known or can be obtained independently. Thus, the gauge cell fluid serves as a reference. We allow mass exchange between the cells; however, the cell volumes are kept unchanged. The conditions of isothermal equilibrium imply the equality of chemical potentials in the pore fluid and in the reference fluid. The limited capacity of the gauge cell constrains the density fluctuations in the pore and allows one to keep the fluid in the pore in a state, which would be unstable in contact with the bulk. In order to stabilize an unstable state, one has to choose the gauge cell of a sufficiently small volume [2]. Thus, the use of the gauge cell has two functions: *to suppress the development of density fluctuations and nucleation and to measure the chemical potential in the pore fluid*. The chemical potential m is related to the pressure in the equilibrium bulk fluid via the bulk equation of state. In this work, we used the equation of state for the LJ fluid developed by Johnson et al [7].

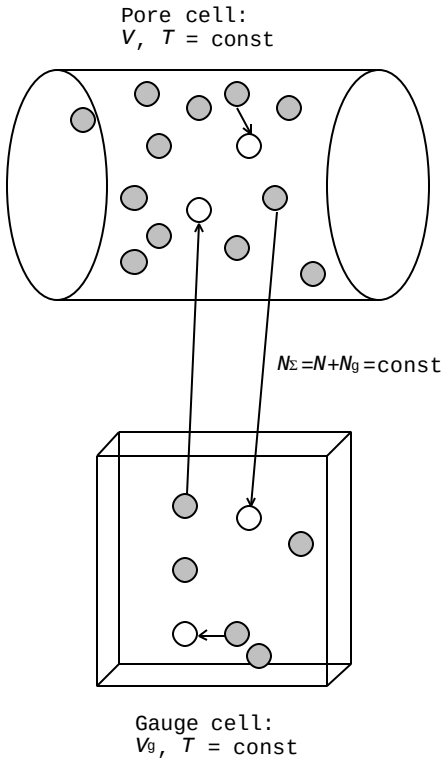

Figure 1. MC simulations in the gauge cell method. The pore cell and the gauge cell of a constant volume are kept in thermal and chemical equilibrium. The allowed types of Monte Carlo steps are (1) displacement of a molecule within the same cell (2) transfer of a molecule between the cells.

LJ parameters s_{ff} = 0.3651nm. e_{ff}/k = 101.5K from ref. [5] were used for nitrogen in MC simulations. The fluid–fluid potential was truncated and shifted at $5s_{ff}$. Solid–fluid parameters were taken from ref. [8]: s_{sf} = 0.317nm, $r_s e_{sf}/k$ = 2253K/nm^2. The typical length of a gauge cell MC simulation was about 10^5 steps per molecule; the final results were obtained by averaging over the last $5*10^4$ MC steps per molecule. Due to the cylindrical shape of the pore, in the MC simulations periodic boundary conditions were applied in the direction parallel to the pore wall. The length of the basic simulation cell was $10s_{ff}$. As for the gauge cell, we employed a cube with triply periodic boundary conditions. The linear size of the gauge cell was at least $40s_{ff}$ and was adjusted so that the sufficient number of fluid molecules was contained in the gauge cell during the simulation. The number of the molecules in the reference cell varied from 40 to 150.

In Figure 2, we present the adsorption isotherm constructed by the gauge cell method. The ascending, adsorption branch OS_v represents the formation of the adsorbed film on the pore walls as the vapor pressure in the bulk increases. Since the fluid in the pore center has a density close to that of vapor, these states are referred to as *vaporlike* states. The adsorption branch

terminates at the *vaporlike spinodal* S_V where the isothermal compressibility diverges. The vaporlike spinodal corresponds to the true limit of stability of the adsorbed film. The descending, desorption branch HS_L describes the decrease of the condensed fluid density as the vapor pressure in the bulk decreases. These states are referred to as *liquidlike* states. The desorption branch terminates at the *liquidlike spinodal* S_L. The liquidlike spinodal corresponds to the true limit of stability of the condensed fluid. The spinodals are connected by the trajectory of physically unstable states, which are stabilized in the simulation by the restrictions of the fluid density in the pore, imposed by the gauge cell, and by the periodic boundary conditions imposed in the lateral direction. A possibility to achieve the true limits of stability of the simulated phases and to determine contiguously the chemical potential distinguishes the gauge cell method as the unique tool to study metastable states and spinodal transitions.

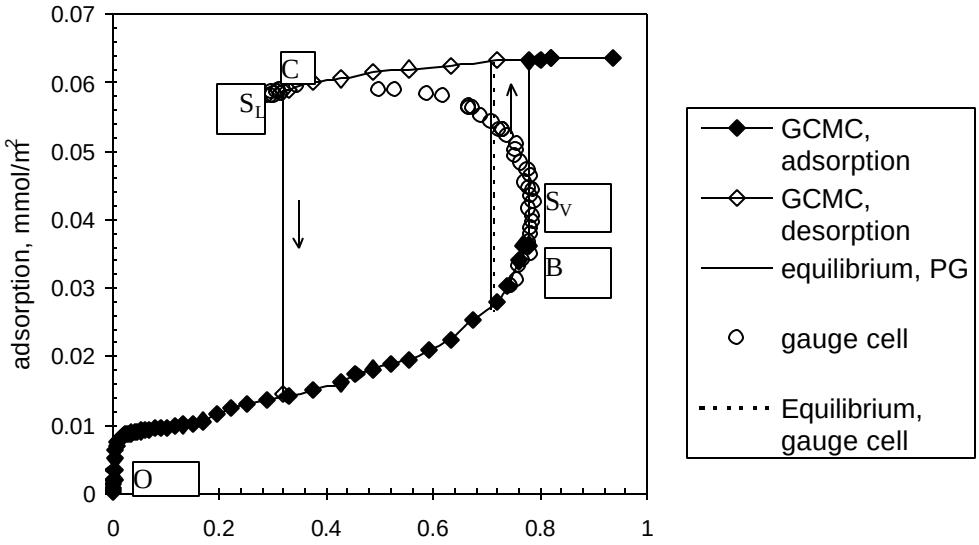

Figure 2. Nitrogen adsorption sotherms in 9.28nm cylindrical silica pore at 77.4K obtained using the gauge cell method and GCMC. Points SV and SL denote vaporlike and liquidlike spinodals, B and C denote locations of spontaneous capillary condensation and evaporation in GCMC simulations, correspondingly.

Vapor–liquid equilibrium. The continuity of the isotherm produced by the gauge cell method allows us to calculate the grand thermodynamic potential $\Omega(m)$ in all states along the isotherm by the integration of the Gibbs equation, $d\Omega = -N\,dm$. The equilibrium chemical potential m_e is determined from the condition of equality of the grand potentials in the vaporlike and liquidlike phases. Thus, the condition of vapor-liquid equilibrium comes to the Maxwell rule of equal areas:

$$\int_{m_e}^{m_{sv}} N_a(m,T)dm - \int_{m_{sl}}^{m_{sv}} N_n(m,T)dm + \int_{m_{sl}}^{m_e} N_d(m,T)dm = 0 \qquad (1)$$

Comparison with GCMC simulations. In Figures 2 and 3, we present also the results of GCMC simulation. The equilibrium states generated by GCMC coincide with those generated by gauge cell method within a statistical error inherent to MC simulations. However, the GCMC adsorption branch terminated at point **C**, where the fluid underwent spontaneous capillary condensation. The point of spontaneous condensation differs somewhat from the vaporlike spinodal $\mathbf{S_V}$, which is achieved in the gauge cell method. Similarly, the GCMC desorption

branch terminated at point **B**, where the fluid underwent spontaneous evaporation prior to the liquidlike spinodal point $\mathbf{S_L}$ achieved by the gauge cell method. In order to determine the phase equilibrium from the GCMC data we performed additional simulations in the supercritical region to circumvent the spontaneous transitions by a continuos trajectory of equilibrium states and performed the thermodynamic integration as recommended by Peterson and Gubbins (PG method) [9]. The results of the thermodynamic integration along the continuous isotherm in the gauge cell method and along the GCMC isotherms connected through the supercritical region are presented in Figure 3. The isotherms for the adsorption branch are in excellent agreement due to the agreement between the adsorption isotherms obtained using GCMC and the gauge cell method. Some discrepancy between the desorption branches of the isotherms for grand potential is related to inherent errors of thermodynamic integration due an arbitrary choice of the integration path. Numerical stability of thermodynamic integration along different paths is discussed in ref. [2]. It appears that the integration along the continuous sigmoid isotherm is more stable numerically than the integration method of ref. [9]. Nevertheless, the two isotherms of the grand potential are in satisfactory agreement (Figure 3).

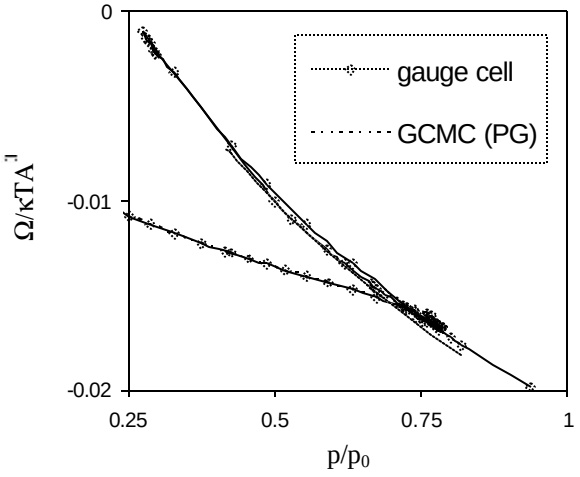

Figure 3. The grand potential isotherms for nitrogen in 9.28nm cylindrical pore at 77.4K obtained using the gauge cell method and the Peterson–Gubbins (PG) method of thermodynamic integration based on GCMC simlations. Arrows show the locations of spontaneous condensation and evaporation in the GCMC simulation.

3. Canonical Ensemble Density Functional Theory (CEDFT).

CEDFT model. In contrast to the conventional Density Functional Theory (DFT), which implies the grand canonical ensemble minimization at given volume, temperature and chemical potential [10], we find equilibrium states of a fluid within a pore of a given shape/volume provided that the mean fluid density, $\langle r \rangle$, is fixed and the system is embedded in a bath of constant temperature *T*. Thus, we deal with a closed system at isothermal conditions, whose equilibrium states are defined by minimization of the Helmholtz free energy, represented as a functional $F[r(\mathbf{r})]$ of the spatially varying fluid density $r(\mathbf{r})$, in the canonical ensemble at constant $\langle r \rangle$, *V*, and *T*. The solution gives the equilibrium density profile $r(\mathbf{r}, \langle r \rangle, T)$ and the chemical potential $m(\langle r \rangle, T)$, of the corresponding state [4]. The CEDFT, as well as the grand canonical DFT, yields the grand potential $\Omega(\langle r \rangle, T)$, which is used to determine the vapor–liquid equilibrium. The adsorption isotherms and the grand potential for stable and metastable states obtained by DFT in the canonical and grand canonical ensembles are practically identical, but CEDFT allows one scan also unstable equilibrium states. Thus, the CEDFT method gives the

conditions of criticality, phase coexistence and spinodal transitions. Several lattice and off-lattice versions of DFT in the canonical ensemble have been reported recently [11-14]. In Figure 4, we present the CEDFT isotherm calculated by minimization of the non-local density functional given by Tarazona's smooth density approximation (for a detail description of this approach, see [15]. The fluid–fluid parameters for the CEDFT model, $s_{ff} = d_{HS} = 0.3575$nm, $e_{ff}/k = 94.45$K (d_{HS} is the hard core diameter), were taken from ref. [16]. The CEDFT parameters differ from those used in the MC simulations due to the differences in the bulk diagrams predicted by the DFT and MC methods (see discussion in refs. [5,15]).

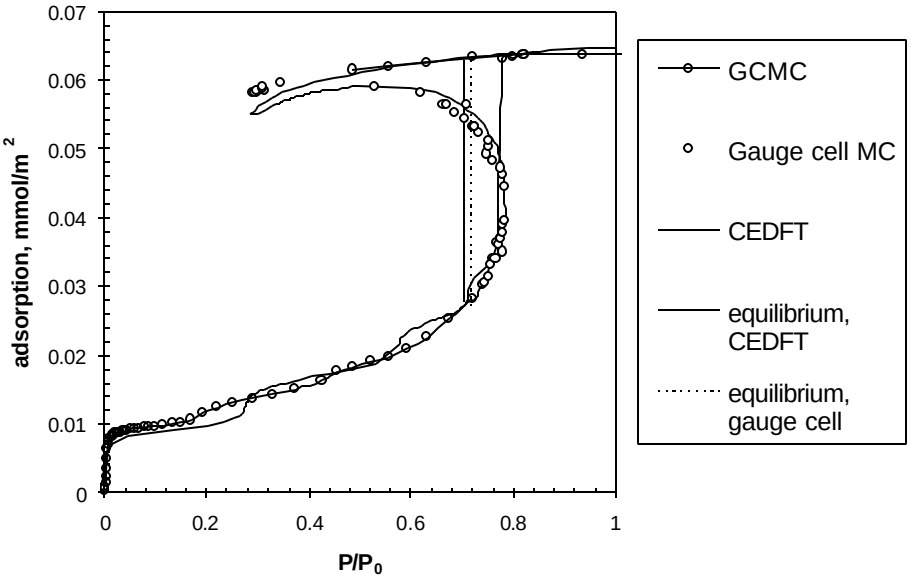

Figure 4. Nitrogen adsorption isotherms in 9.28nm cylindrical silica pore at 77.4K obtained using the gauge cell method and CEDFT

Comparison of CEDFT and MC simulations. In Figure 4, we compare the CEDFT and MC isotherms. The CEDFT adsorption isotherm exhibits artificial step-wise layering transitions, which is well understood for a one-dimensional model [15]. However, overall agreement between the MC and DFT adsorption branches is good up to the vaporlike spinodal. Agreement in predicting the vaporlike spinodal pressure is truly remarkable. Because the parameters of both models were chosen to represent the liquid density of bulk nitrogen, good agreement between the MC and CEDFT isotherms is obtained for the desorption branch. Although CEDFT predicts larger compressibility than the gauge cell method in the vicinity of the liquidlike spinodal, agreement of the liquid-like spinodal pressures is excellent. The unstable states located on the backward trajectory are also in remarkable agreement. Note that these translation invariant configurations cannot be observed experimentally and are artificially stabilized in the both models. Despite the unstable trajectories predicted by the two methods deviate somewhat near the vapor-like spinodal (explanation of the peculiar behavior of the phase diagram in this region will be presented elsewhere), the thermodynamic integration along the unstable parts of the isotherms yields satisfactory agreement, as shown in Figures 5.

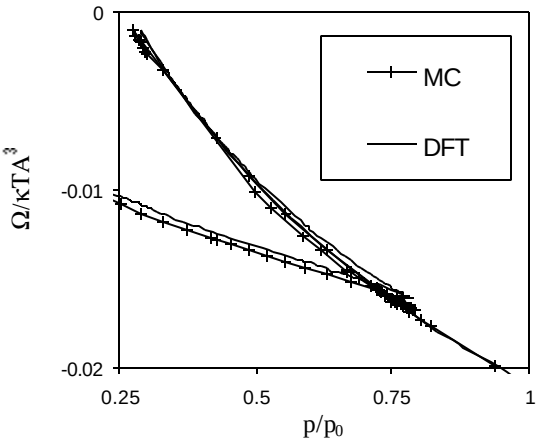

Figure 5 The grand potential isotherms for nitrogen in 9.28nm cylindrical pore at 77.4K obtained using the gauge cell method and CEDFT

4. Comparison of theoretical predictions with experimental data.

In Figure 6, we compare the theoretical adsorption isotherms with the experimental adsorption isotherm measured on a sample of a MCM-41 type material [17]. MCM-41 type materials [18] contain a two-dimensional hexagonal array of cylindrical pores of a predetermined diameter and serve as the best available references for adsorption studies.

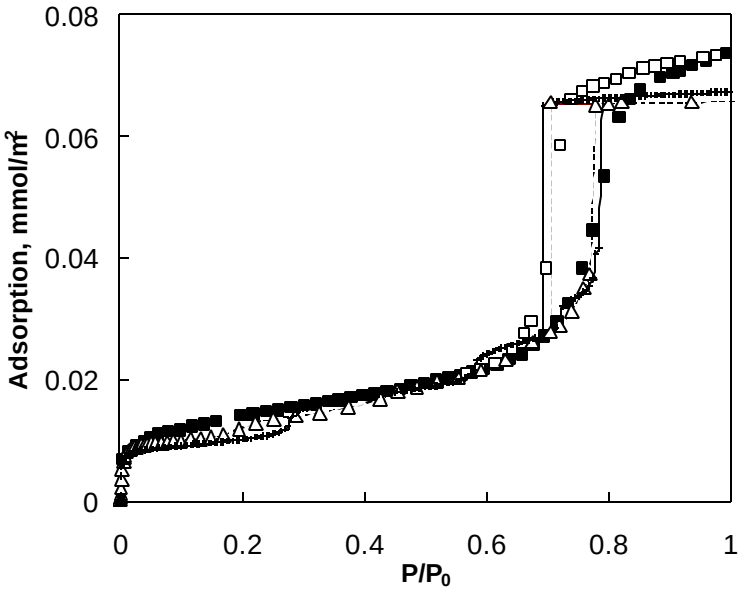

Figure 6. Nitrogen adsorption isotherms on an MCM-41 sample at 77.4K. Experimental data [17], CEDFT calculation, and MC simulation (metastable liquidlike and unstable branches are not shown.

As related to the capillary condensation and evaporation in open-ended cylindrical pores, it is well documented that the metastable liquidlike states are not observed in experiments, since the evaporation occurs at the vapor–liquid equilibrium pressure via the formation of a meniscus at the pore edge [19,20]. At the same time, metastable vaporlike states can be monitored experimentally and therefore condensation may occur irreversibly as a spontaneous transition from a metastable state to a stable state, giving rise to the hysteresis. In the adsorption literature this effect is referred to as “delayed

condensation" [21]. When the delayed condensation occurs close to the vaporlike spinodal, it is said that the condensation proceeds in the regime of developed hysteresis [22]. This case is demonstrated in Figure 6: experimental capillary condensation pressure is very close to the liquid-like spinodal, while the experimental desorption corresponds to the vapor–liquid equilibrium, predicted by the CEDFT and MC methods. Good agreement between the vapor branches of the theoretical and experimental adsorption isotherms was obtained in the region of polymolecular sorption. Appreciable deviations from the experiment were observed only in the monolayer region, since the pore model with an energetically uniform, structureless wall cannot capture the intrinsic molecular heterogeneity of silica surface [23].

5. Conclusions

The gauge cell method and CEDFT are proved to be efficient for the calculation of adsorption isotherms, determination of the conditions of vapor–liquid equilibrium in pores, estimation of the true limits of stability of liquidlike and vaporlike states. The methods allow one to calculate the full sorption isotherm, which at the subcritical conditions has a sigmoid shape similarly to the van der Waals isotherm.

The methods are illustrated on the prominent example of the capillary condensation hysteresis of nitrogen at 77 K in a cylindrical pore of 9.3 nm in diameter. The adsorption isotherms obtained using the gauge cell method agree with the GCMC data. In the vicinity of the vaporlike and liquidlike spinodals, the gauge cell method reveals the states, which are not achieved in GCMC simulations. In particular, the limits of stability of the metastable vaporlike and liquidlike states achieved in the GCMC simulation differ from the true limits of stability represented by the vaporlike and liquidlike spinodals. The conditions of vapor–liquid equilibrium obtained using the gauge cell method through thermodynamic integration along the sigmoid adsorption isotherm agree well with the integration along a subcritical isotherm and a path of constant chemical potential proposed in ref [9]. Good agreement between the MC and CEDFT adsorption isotherms was obtained.

We compared the calculated MC and CEDFT hysteretic isotherms with the experimental data on argon sorption for a sample of mesoporous molecular sieve of MCM-41 type with the characteristic pore diameter of 9.3 nm [17]. We demonstrate a remarkable consistency of the theoretical and experimental isotherms, especially in the region of polymolecular adsorption and at the capillary condensation and desorption steps. The experimental desorption pressure corresponds to the calculated pressure of vapor–liquid equilibrium, while the experimental condenstion pressure corresponds to the predicted pressure of the vaporlike spinodal. This conclusion is limited to the systems with a regular pore structure, such as the MCM-41 type materials, when the pore blocking effects are not appreciable. In disordered materials, as shown on the examples of simulated models of porous glasses and silica gels the hysteretic behavior of adsorption-desorption isotherms is more complicated [24-27].

The gauge cell method and CEDFT are recommended for studies of other equilibrium processes and phase transitions in confined systems such as multicomponent sorption, phase separation, dewetting of thin films, nucleation, and the like.

References

(1) L.D. Gelb, K.E. Gubbins, R. Radhakrishnan, M. Sliwinska-Bartkowiak, *Rep. Prog. Phys.* **1999**, *62*, 1573-1659.

(2) A.V. Neimark, A. Vishnyakov, *Phys. Rev. E* **2000**, *62*, 4611-4622.

(3) A. Vishnyakov, A.V. Neimark, *J. Phys. Chem. B* **2001**, *in press.*
(4) A.V. Neimark, P.I. Ravikovitch In *Microscopic Simulation of Interfacial Phenomena in Solids and Liquids*; S.R. Phillpot, P.D. Bristowe, D.G. Stroud, J.R. Smith, Eds.; Materials Research Society: Warrendale, Pennsylvania, 1998; Vol. 492.
(5) P.I. Ravikovitch, A. Vishnyakov, R. Russo, A.V. Neimark, *Langmuir* **2000**, *16*, 2311-2320.
(6) G.J. Tjatjopoulos, D.L. Feke, J.A. Mann, *J. Phys. Chem.* **1988**, *92*, 4006-4007.
(7) J.K. Johnson, J.A. Zollweg, K.E. Gubbins, *Mol. Phys.* **1993**, *78*, 591-618.
(8) P.I. Ravikovitch, S.C. Odomhnaill, A.V. Neimark, F. Schuth, K.K. Unger, *Langmuir* **1995**, *11*, 4765-4772.
(9) B.K. Peterson, K.E. Gubbins, *Mol. Phys.* **1987**, *62*, 215-226.
(10) R. Evans, U.M.B. Marconi, P. Tarazona, *J. Chem. Phys.* **1986**, *84*, 2376-2399.
(11) L.J.D. Frink, A.G. Salinger The AIChE 2000 Annual Meeting, Los Angeles, 2000.
(12) R.W. Maier, E. Maginn, M.A. Stadtherr The AIChE 2000 Annual Meeting, Los Angeles, 2000.
(13) A.P. Malanoski, F.V. Swol The AIChE 2000 Annual Meeting, Los Angeles, 2000.
(14) G.L. Aranovich, M.D. Donohue, *Phys. Rev. E* **1999**, *60*, 5552-5560.
(15) P.I. Ravikovitch, A. Vishnyakov, A.V. Neimark, *Phys. Rev. E* **2001**, *64*, 0116XX1-0116XX20.
(16) P.I. Ravikovitch, D. Wei, W.T. Chueh, G.L. Haller, A.V. Neimark, *Journal of Physical Chemistry B* **1997**, *101*, 3671-3679.
(17) A. Sayari, M. Kruk, M. Jaroniec, I.L. Moudrakovski, *Adv. Mater.* **1998**, *10*, 1376-+.
(18) C.T. Kresge, M.E. Leonowicz, W.J. Roth, J.C. Vartuli, J.S. Beck, *Nature* **1992**, *359*, 710-712.
(19) D.H. Everett In *The Solid-Gas Interface*; E.A. Flood, Ed.; Marcel Dekker: New York, 1967; Vol. 2.
(20) R. Evans, *J. Phys.-Condes. Matter* **1990**, *2*, 8989-9007.
(21) K.S.W. Sing, D.H. Everett, R.A.W. Haul, L. Moscou, R.A. Pierotti, J. Rouquerol, T. Siemieniewska, *Pure Appl. Chem.* **1985**, *57*, 603-619.
(22) A.V. Neimark, P.I. Ravikovitch, A. Vishnyakov, *Phys. Rev. E* **2000**, *62*, R1493-R1496.
(23) M.W. Maddox, J.P. Olivier, K.E. Gubbins, *Langmuir* **1997**, *13*, 1737-1745.
(24) E. Kierlik, M.L. Rosinberg, G. Tarjus, P. Viot, *Phys. Chem. Chem. Phys.* **2001**, *3*, 1201-1206.
(25) L. Sarkisov, P.A. Monson 7th international conference on Fundamentals of Adsorption, Nagasaki, Japan, 2001; p P-061.
(26) L. Gelb, K.E. Gubbins 7th international conference on Fundamentals of Adsorption, Nagasaki, Japan, 2001; p P-056.
(27) R.J.M. Pelleq, P. Levitz 7th international conference on Fundamentals of Adsorption, Nagasaki, Japan, 2001; p P-064.